ELSEVIER

Contents lists available at ScienceDirect

# Journal of Arid Environments

journal homepage: www.elsevier.com/locate/jaridenv





# Determining the response of riparian vegetation and river morphology to drought using Google Earth Engine and machine learning

Smriti Chaulagain <sup>a,\*</sup>, Mark C. Stone <sup>a</sup>, Ryan R. Morrison <sup>b</sup>, Liping Yang <sup>c,d,e</sup>, Julie Coonrod <sup>a</sup>, Noelani E. Villa <sup>a</sup>

- a Department of Civil, Construction, and Environmental Engineering, University of New Mexico, Albuquerque, NM, 87131, USA
- <sup>b</sup> Department of Civil and Environmental Engineering, Colorado State University, Fort Collins, CO, 80523-1372, USA
- <sup>c</sup> Department of Geography and Environmental Studies, University of New Mexico, Albuquerque, NM, 87131, USA
- d Center for the Advancement of Spatial Informatics Research and Education (ASPIRE), University of New Mexico, Albuquerque, NM, 87131, USA
- <sup>e</sup> Department of Computer Science, University of New Mexico, Albuquerque, NM, 87106, USA

#### ARTICLE INFO

# Keywords: Riparian vegetation River morphology Remote sensing Random forest Rio Grande Drought

#### ABSTRACT

Riparian vegetation composition and channel morphology are susceptible to long-term alterations caused by external stressors, including climate-change-induced droughts and engineered infrastructures. The objectives of this study were to (1) quantify trends in riparian vegetation and channel/floodplain morphology over large spatial (~290 km) and temporal scales (~30 years) and (2) investigate the relationships between hydroclimatic drivers and changes in riparian vegetation and channel morphology. We implemented a random forest classifier via a machine learning technique in Google Earth Engine. The study area was a 290 km reach of the Rio Grande located in New Mexico, USA. We used the combination of remotely sensed data and products (e.g., Landsat imagery, Normalized Difference Vegetation Index (NDVI), and land cover) to characterize vegetation, vegetation cover changes, and river morphology shifts from 1984 to 2020. The trend analysis revealed increased vegetated areas and NDVI (0.0004/yr) during long-term drought. The channel experienced a reduction in width associated with vegetation encroachment and the formation of stable vegetated islands. The streamflow hydrograph characteristics were positively correlated with vegetation cover and channel morphology. Our study contributes novel insights into the long-term riparian ecosystem dynamics under drought stress, informing drought impact mitigation and ecosystem management in arid and semi-arid regions.

#### 1. Introduction

In semi-arid regions such as the Southwestern United States (USA), rivers are experiencing pressure due to drought-induced streamflow alterations, increased water demand, changes in land use, and engineered structures (e.g., dams, levees, etc.) (Poff et al., 2007). River engineering projects disturb natural sediment transport processes (Bollati et al., 2014). Artificial levees impact floodplain connectivity by limiting the active floodplain and changing the original flow path of the channel (Knox et al., 2022). These disturbances affect the riparian vegetation and the river geomorphology (Stromberg et al., 2010). Consequently, ecosystem services provided by the river system are deteriorating in many river systems, particularly in semi-arid regions.

Besides providing ecosystem services, vegetation alters river

hydraulics by adding resistance to the flow and reducing bed shear stress (Nepf, 2012). Vegetation also affects the forms and dynamics of channel morphology, such as alteration of channel width, formation of stable islands, and reduction in braiding intensities (Gurnell et al., 2001). Furthermore, changes in river hydrology, geomorphology, and riparian vegetation have cascading impacts on other aspects of the river corridor system, including hydrological connectivity, sediment regimes, and habitat provisioning (Brierley et al., 1999). These changes are sensitive to the hydroclimatic components (streamflow and climatic conditions) that vary from seasons to decades in addition to climate variability (Yonaba et al., 2021a). Thus, understanding the interactions of these components in response to external drivers of change is essential for advancing river conservation and management. Long-term observation can help river managers to understand the response of vegetation and

<sup>\*</sup> Corresponding author. University of New Mexico, Albuquerque, NM, 87131, USA.

E-mail addresses: schaulagain@unm.edu, cha.smriti@gmail.com (S. Chaulagain), stone@unm.edu (M.C. Stone), ryan.morrison@colostate.edu (R.R. Morrison), lipingyang@unm.edu (L. Yang), jcoonrod@unm.edu (J. Coonrod), noelv@unm.edu (N.E. Villa).

channel morphology due to these external drivers.

Usually, riparian vegetation is monitored through indicators of succession, species composition (native or invasive species), vegetation structure (height, density, biomass), and physiological processes (health status, phenology, evapotranspiration) (Nagler et al., 2016). The changes in channel morphology have been studied and quantified by comparing channel topography, observing patterns in aerial imagery (Swanson et al., 2011), through numerical approaches (e.g., BASEMENT software) (Artini et al., 2021), and using physical models (Bertoldi et al., 2015). Traditionally, topographic data are collected from field measurements at different periods to determine the changes in channel geometry. However, due to the spatial variability and dynamics of vegetation and morphology, field data collection is challenging, labor-intensive, expensive, and time-consuming, making this approach impractical for large study areas (>100 km) and multiple years (Johansen et al., 2010). Remote Sensing (RS) approaches offer a cost-effective way to monitor the vegetation and morphology over large spatial domains for extended temporal scales.

Remote sensing products, especially satellite imagery (e.g., Landsat, Sentinel, and MODIS), are widely used in determining changes in riparian vegetation and channel morphology (Isikdogan et al., 2017; Langat et al., 2019; Monegaglia et al., 2018). Most of the techniques rely on spectral indices such as the Normalized Difference Vegetation Index (NDVI), Normalized Difference Water Index (NDWI), Modified NDWI (MNDWI), or simply by classifying images for delineating the wetted channel and vegetation. NDVI is the most common indicator to monitor vegetation impacts from climate trends and changes in streamflow. NDVI represents photosynthetic activity, which is directly related to climatic conditions (Ndayisaba et al., 2017) and water availability (Sims and Colloff, 2012). Additionally, satellite images are used to extract morphodynamics for either single or multithreaded channels with the capacity to delineate surface water (Isikdogan et al., 2017), complex features such as emerging bars (Monegaglia et al., 2018), and deposition or erosion patterns (Langat et al., 2019). These studies utilized either manual (Han et al., 2020), semi-automatic (Schwenk et al., 2017), or fully automatic (Monegaglia et al., 2018) approaches to delineate open water surface advancing from simple algorithms (Langat et al., 2019) to deep learning algorithms (Isikdogan et al., 2017). However, such studies are limited in terms of spatial and temporal scale, i.e., discrete analysis ranging from seasons to decades. Moreover, large spatiotemporal scale studies are challenging due to the limited data availability and processing of large datasets.

The emergence of cloud-based storage and computing platforms such as Google Earth Engine (GEE) (Gorelick et al., 2017) has enabled researchers to undertake long-term, large-scale monitoring of vegetation and channel morphology. Prior studies have implemented GEE for spatiotemporal analysis of riparian vegetation and channel morphology (Boothroyd et al., 2021a; Boothroyd et al., 2021b; Pu et al., 2021). Boothroyd et al. (2021a) performed a spatiotemporal analysis of channel morphology and riparian vegetation using NDWI and NDVI within GEE cloud-based computing platform for a single-threaded, meandering channel. Similarly, Pu et al. (2021) assessed riparian vegetation and channel morphology in terms of NDVI and MNDWI using high-resolution National Agriculture Imagery Program (NAIP) imagery in GEE.

The mechanism and local effects of vegetation and hydrological variables on morphology are well documented. Numerous studies focused on determining the relationship between the NDVI and climate variables (Chi et al., 2020; Weiss et al., 2004). Some studies investigated the spatiotemporal trends of hydrological variables with riparian vegetation and channel morphology (Caruso et al., 2013; Picco et al., 2017). Despite prior studies, there is still a gap in our knowledge regarding interrelated responses of riparian vegetation and channel morphology at a large spatiotemporal scale.

The response of riparian vegetation to long-term droughts in an arid region, its cascading impacts on the other aspects of the river system,

and the study of the complex interaction between the vegetation, morphology, and hydroclimatic variables are the emerging topics of interest in the present context. This research aimed to enhance the understanding of riparian vegetation and channel morphology responses to external drivers of change (hydroclimatic variables) using ML on a large spatiotemporal scale, especially for the semi-arid region. The objectives of this research were to (1) quantify trends in riparian vegetation and channel/floodplain morphology over large spatial (~290 km) and temporal scales (~30 years) and (2) investigate the relationships between hydroclimatic drivers and changes in riparian vegetation and channel morphology. This study used NDVI (1984–2020) and land cover (LC) maps to determine the spatiotemporal changes of vegetation and channel morphology for a 290 km reach of the Rio Grande in New Mexico, USA.

#### 2. Methods

#### 2.1. Study area

This study focused on a 290 km reach of the Rio Grande in New Mexico, USA (Fig. 1). The study reach extends from Cochiti Dam to Elephant Butte Reservoir. This reach is also known as the Middle Rio Grande (MRG). The MRG is a heavily regulated, physically modified, snowmelt-dominated river, with the highest discharges occurring in May and June. The dominant native vegetation species along the MRG include cottonwood (*Populus deltoids*) and coyote willow (*Salix exigua*). Non-native vegetation species includes salt cedar (*Tamarix ramosissima*) and Russian olive (*Elaeagnus angustifolia*) (Mussetter Engineering Inc., 2006).

The MRG has gone through several modifications across different eras. From the 1930s to the 1950s, spoil-bank levees derived from the excavation of riverside drains were constructed for flood protection along both banks, disconnecting the river from its historical floodplains. From the 1950s to the 1970s, engineered levees replaced the spoil banks, and an equi-width (180 m) channel controlled by jetty jack fields were constructed within the levees to improve downstream flow conveyance and reduce flood risk. Cochiti Dam has regulated the streamflow at the head of the reach since 1973. Four other low-head diversion dams along the reach divert water for irrigation (Angostura, Isleta, and San Acacia dams) and municipal water supply (Albuquerque drinking water diversion) with no flood control capacity.

Due to an extended drought since 2000 (Petrakis et al., 2017), a reduction in discharge has caused a narrowing of the channel, formation of new bars and islands with stable vegetation, sediment aggradation, and bank undercutting (Swanson et al., 2011). This reach also consists of several river restoration projects implemented to recover the Federally listed endangered Rio Grande silvery minnow (*Hybognathus amarus*) and southwestern willow flycatcher (*Empidonax traillii extimus*). Some portions of the riparian zone, especially the over-aged cottonwood gallery forests that were initially established by floods in the 1940s, have been impacted by wildfires in the past two decades.

Here, the study reach is divided into four sub-sections based on the availability of validation datasets for sub-reaches (Fig. 1). The reach from Cochiti dam to Alameda bridge is considered the *Upstream reach*; Alameda bridge to Isleta dam is referred to as the *Albuquerque reach*; Isleta dam to San Acacia dam is the *Isleta reach*; and San Acacia dam to San Marcial is the *San Acacia reach*.

# 2.2. Data processing

The sequence of methodologies followed for preprocessing images and data analysis is represented in Fig. 2. The datasets used in this study are summarized in Table A1 (Appendix). The images were processed by removing the shadows and clouds from Landsat images. The NDVI was calculated from preprocessed images. Sample datasets were created for the RF classification. The validated LC was overlaid with the NDVI to

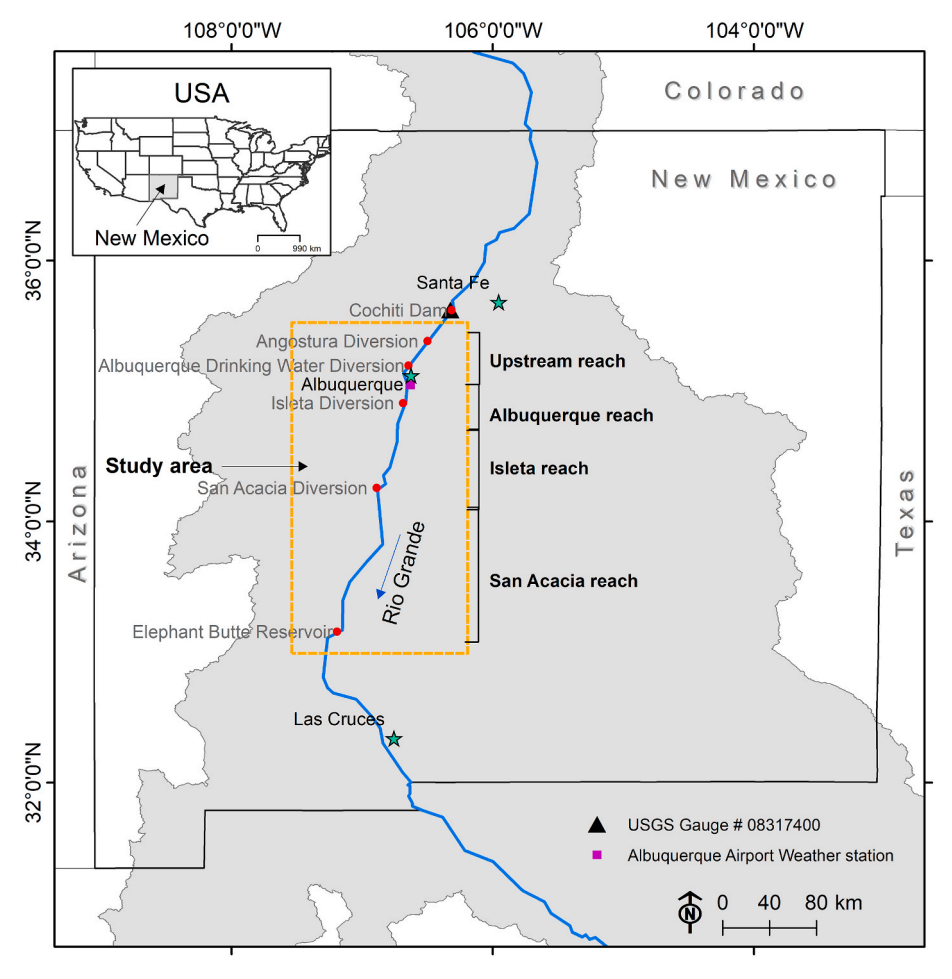


Fig. 1. Study area located between Cochiti Dam and Elephant Butte Reservoir.

determine the spatiotemporal trends of vegetation and morphology. Finally, hydroclimatic variables were correlated with NDVI and channel width to determine the spatiotemporal correlation between these variables.

#### 2.2.1. Image collections

This study used multi-spectral and multi-temporal satellite imagery, Landsat images, collected by sensors Landsat 5, 7, and 8 from 1984 to 2020 (37 years). Landsat 5 Thematic Mapper imagery data are available from 1984 to 2011; Landsat 7 Enhanced Thematic Mapper data from 1999 to the present; and Landsat 8 Operational Land Imagery from 2013 to the present. Landsat 7 data contains gaps between the images due to scan line errors, which require correction to fill gaps with gap mask files. Due to data limitations, Landsat 7 data was used for 2012 only. The spatial resolution for these images is 30 m, collected every 16 days. For Landsat 1 to 4, images are available from 1972, but the spatial resolution is more than 30 m.

The trends for riparian vegetation and channel morphology were investigated from May to August (growing season). The mean monthly NDVI (Figure A1, Appendix) was higher from May to August compared to other months of the year. The study region is arid to semi-arid, which is beneficial for obtaining images with less cloud cover (mostly <10%) during those months. The Landsat images from the GEE cloud-based storage were used. First-tier surface reflectance Landsat products available from the GEE data catalog are atmospherically corrected, which is one of the advantages of using GEE.

# 2.2.2. Preprocessing of images

The image collections were filtered over the growing season in the

GEE cloud-based computing platform. Using the Landsat World Reference System, images were extracted and processed for paths 33 and 34 and rows 35 to 37. The study area contains 1532 tiles of images for the growing season. Clouds and shadows were masked out using the function available in GEE API. The resulting images preserve the metadata and footprint of input images, while areas transitioning from zero in the mask are filled with zeros or values close to zero within the range of pixel type (Gorelick et al., 2017). The images were aggregated using the median function as a reducer to obtain annual time series images; instead of the mean function for higher accuracy (Phan et al., 2020).

## 2.3. Vegetation trend analysis

NDVI was used for long-term monitoring of vegetation. NDVI (NIR-R/R + NIR) depends on the red (R) and near-infrared (NIR) spectral bands. NDVI was calculated using JavaScript from the preprocessed images in the GEE code editor. NDVI values < 0.2 were masked out to identify vegetation only (Yonaba et al., 2021b). The mean monthly NDVI to investigate the seasonal variation in greenness and the mean annual NDVI for the growing season were determined. Growing season NDVI for sub-reaches was also determined to analyze spatial NDVI trends.

Simple linear regression does not perform well for data affected by seasonality (Assal et al., 2021) for determining trends. Therefore, a non-parametric Mann-Kendall test was performed to determine the trends in NDVI using a Python package called *pymannkendall* (Hussain and Mahmud, 2019). This package includes the modified Mann-Kendall test addressing autocorrelation by a variance correction approach (Hamed and Ramachandra Rao, 1998). A p-value of 0.05 was used to

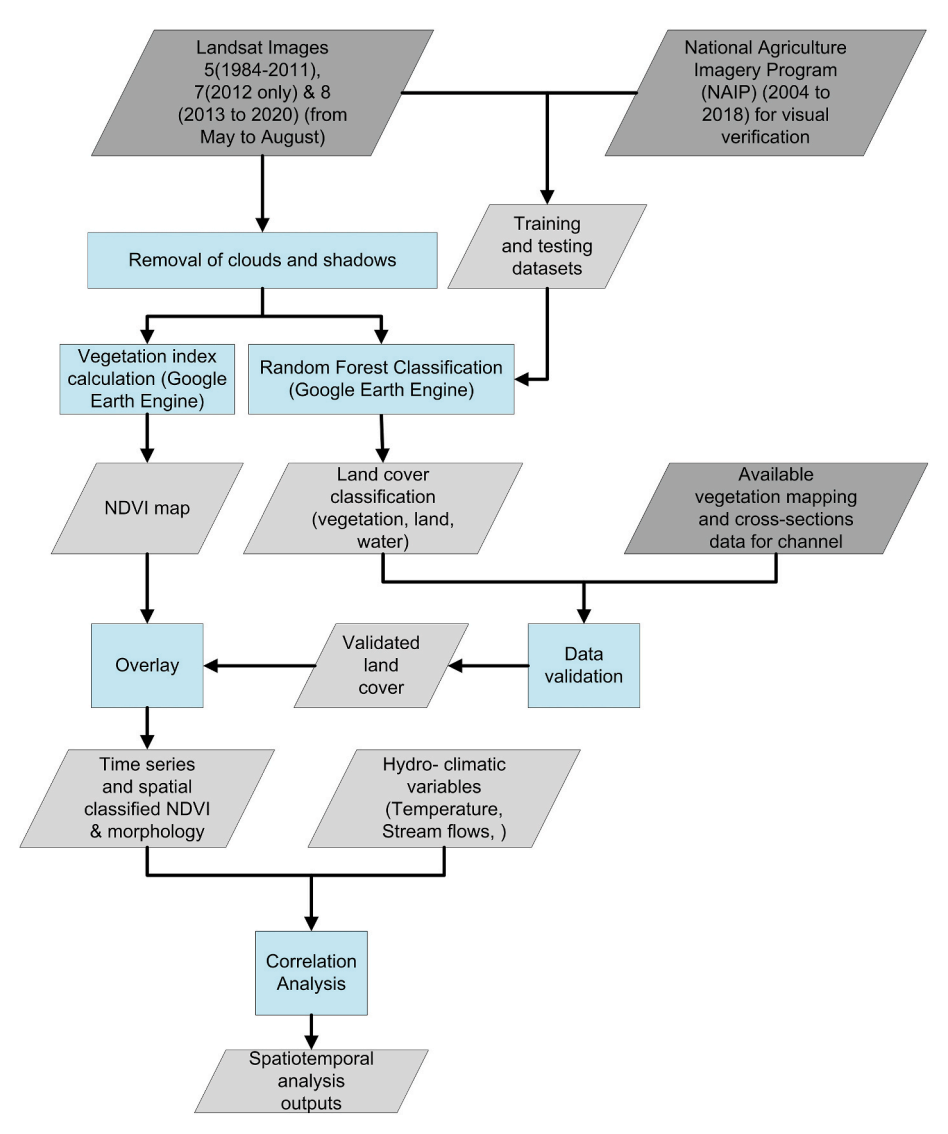


Fig. 2. Flow chart summarizing the methods. Blue is coded for the processes performed, and light grey represents the input/output datasets. Dark grey represents the available datasets from external sources.

check the significance of the trend. Also, the trend in NDVI for an extended time may not always follow monotonic change. Due to external disturbances such as flooding and drought events, abrupt changes in the greenness of vegetation can occur. To address these issues, trend breakpoints were detected manually (Assal et al., 2021).

The period from 1984 to 1999 was categorized as drought, and 2000 to 2020 as a non-drought period based on the study of Petrakis et al. (2017) for further analysis. Palmer Drought Severity Index was used in their study to determine the drought period.

# 2.4. LC mapping

LC maps were created from the Landsat Images to observe vegetation status and channel morphology changes. LC classification was performed using the built-in RF algorithm based on supervised image classification within the GEE. The RF algorithm was selected because of its robustness and accuracy, especially for LC classification (Yang and Cervone, 2019).

The sampling datasets (training and testing) were created manually to train the data for supervised classification. LC classification was performed every two years with the assumption of less chance of change in vegetation and morphology unless affected by extreme external stressors (e.g., floods, wildfires). The datasets were visually verified for

2009, 2011, 2014, 2016, and 2018 with the available NAIP imagery. The ratio of sampling data was created according to the best judgment of the study area to avoid data imbalance issues. The average number of sampling points ranged from 200 to 500 for each class. The sampling datasets were randomly split into training (80% data) and testing (20% data) datasets. Training datasets were used for the classification of images, and the testing datasets were used to check the model's overall accuracy (OA). LC was classified into three classes: bare land, water, and vegetation. The riparian zone of the study area does not contain significant areas of infrastructure such as buildings or other LC types. LC maps were exported from GEE cloud storage for further analysis.

The channel morphology was analyzed by estimating the channel width from LC. The channel width was obtained by counting the pixels classified as water. The pixels on the channel islands identified with vegetation were not included in determining channel width.

The two major parameters for RF algorithm are the *number of decision* trees and the *number of features/variables* to consider for best splitting. Based on previous studies, 100 decision trees were selected (Maxwell et al., 2019). The number of features/variables used for splitting was considered the default value (e.g., the square root of the total number of input features).

Two commonly used matrices (OA and F1-score) were employed to determine the LC accuracy (Foody, 2020). OA represents the proportion

of correctly classified classes (Türk, 1979). F-measure (F1- score, equation (2)) measures the model's accuracy based on the harmonic mean from precision (equation (3)) and recall (equation (4)) calculated from binary confusion matrices.

$$OA = \frac{True \ positive \ (TP) + True \ negative \ (TN)}{TP + TN + False \ negative \ (FN) + False \ positive \ (FP)} \tag{1}$$

$$F1 - score = \frac{2Precision \times Recall}{Recall + Precision}$$
 (2)

$$Precision = \frac{TP}{TP + FP} \tag{3}$$

$$Recall = \frac{TP}{TP + FN} \tag{4}$$

#### 2.5. Validation datasets

The vegetated area obtained from the ML technique was compared with the vegetation mapping prepared originally by Hink and Ohmart (1984) and repeated several times in successive years. Those vegetation maps were prepared by verification from field observations and aerial photographs. The data are available periodically between 1984 and 2016 and cover the specific reach for a specific time.

The changes in channel width determined from ML were also verified by comparing with surveyed cross-section data collected by the United States Bureau of Reclamation (USBOR), Albuquerque Area Office. USBOR contractors surveyed fixed cross-sections on a frequent basis (every two to three years).

#### 2.6. Hydroclimatic variables

The hydroclimatic variables used in this study were temperature, precipitation, estimated reference evapotranspiration, and streamflow. Meteorological variables collected at the Albuquerque Airport (ABQ) were used. This station was selected because it lies in the middle of the study reach. Streamflow data from USGS Gauge 08317400, below Cochiti Dam was used. This gauging station was chosen because it represents the overall streamflow patterns.

From the streamflow data, flood frequency, duration, timing, and magnitude were analyzed from 1980 to 2020 using the Indicators of Hydrologic Alteration (IHA) software package. IHA calculates 33 hydrological alterations and 34 environmental flow components (Richter et al., 1996) based on ecosystem influences such as soil moisture availability for vegetation and habitat for aquatic organisms. Streamflows were categorized into extremely low flows (<10 percentiles of daily flows), low flows (<75%), and high flows (>75%). High flows were further classified as small (>2 years return period of high flows) and large floods (10 years return period of high flows). Depending on the section of the study reach, the floodplains start to inundate after discharge exceeds 57–142 m³/s. The parameters such as high and low flow frequency and high and low pulses influence the recruitment of vegetation and the dynamics of the river system, which were used for further analysis.

# 2.7. Correlation between vegetation, morphology, and hydroclimatic variables

Spearman's Rank correlations were calculated to determine the relationships between vegetation, morphology, and hydroclimatic variables. Mean Decrease Impurity (MDI), one of the widely used measures for selecting features (Calle and Urrea, 2011), was used to determine the important hydroclimatic variables that impact the dependent/target variable (NDVI for vegetation and channel width for morphology). MDI determines the importance of each variable by evaluating the change in prediction (Calle and Urrea, 2011). The higher MDI value means the

variable's importance is higher for predicting a target variable.

#### 3. Results

#### 3.1. LC classification accuracy

OA and F1-score were calculated to evaluate the performance of RF for LC classification. OA was >95% for water, land, and vegetation classes. F1-score was also >85% for each category. The classified images were also visually verified using high-resolution NAIP imagery before calculating these matrices.

#### 3.2. Validation datasets

The vegetated area determined from RS techniques closely matched the ground-truth data for the Albuquerque reach (Table 1). However, LC from ML slightly underestimated the vegetated area compared to ground-truth data for most conditions in other sub-reaches.

The relationship of channel width obtained from the ML and USBOR surveyed cross-sections is shown in Fig. 3. The analysis reveals close agreement between RS and field measurements of channel width ( $R^2=0.9942)$  with a small underestimation from ML compared to the survey data.

#### 3.3. Temporal analysis of vegetation and morphology

Between 1980 and 2020, riparian vegetation changed both in temporal and spatial extent. The statistical summary of NDVI for the growing season is represented by a box plot (Fig. 4). Fig. 4 reveals the wider ranges (0.2–0.9) of NDVI over time. The analysis was limited to NDVI >0.2. As a result, the minimum value is equal to 0.2.

The growing season mean NDVI for the study reach is shown in Fig. 5 (A). NDVI fluctuated from 1984 to 2000, with the lowest value in 1996. NDVI was relatively low from 2000 to 2010 and increased from 2010 to 2020. This pattern was similarly observed for the sub-reaches (Fig. 5B). However, NDVI for the Upstream reach was lower, and the Albuquerque reach had higher NDVI until 2000 than the other sections. The Isleta reach also experienced higher NDVI for the study period.

A non-parametric Mann-Kendall test was performed to investigate temporal trends (Fig. 5 (A)). This test indicated no significant (p < 0.05) monotonic trend for the entire study period. The annual increase of 0.0004/yr was observed. To observe the dynamics of vegetation, trends were analyzed by considering breakpoints manually. The trend analysis shows that there was no significant monotonic trend (p < 0.05) from 1984 to 1987 (p=1.0), a significant increasing trend from 1987 to 1995 (p=0.047), a significant decreasing trend from 1995 to 2006 (p=0.02), and again a significant increasing trend from 2006 to 2020 (p=0.0045). The annual increase in NDVI from 1987 to 1995 was 0.0065/yr. An annual decrease of 0.0062/yr was observed from 1996 to 2006. An annual increase of 0.005/yr was observed from 2006 to 2020.

**Table 1**Comparison of the vegetated area between the ML technique and the vegetation mapping prepared by Hink and Ohmart (1984).

Year	Sub-Reach	Area from ground-truthing (km²)	Area from ML (km²)	Percentage differences between ground-truth and ML
2003	San Acacia	48.35	40.26	16.7%
2016		51.13	52.22	-2.13%
1984	Albuquerque	11. 63	11.61	0.17%
2005		10.34	10.17	1.64%
1984	Isleta	30.69	23.14	24.6%
2003		31.57	27.15	14%
2016		36.26	32.61	10%

(Positive values mean the ground-truth overestimated the vegetated area compared to ML).

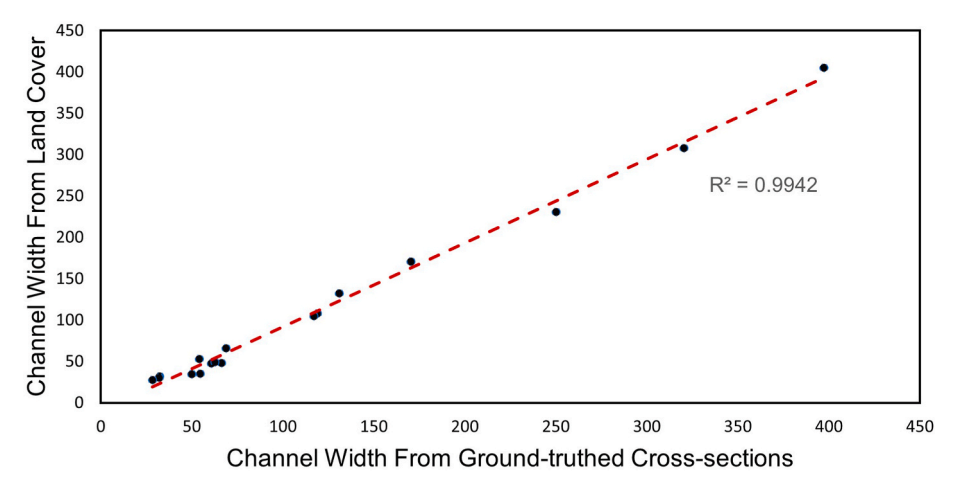


Fig. 3. Relationship of channel width from machine learning (Landsat derived LC) and cross-sections measured by United States Bureau of Reclamation, Albuquerque.

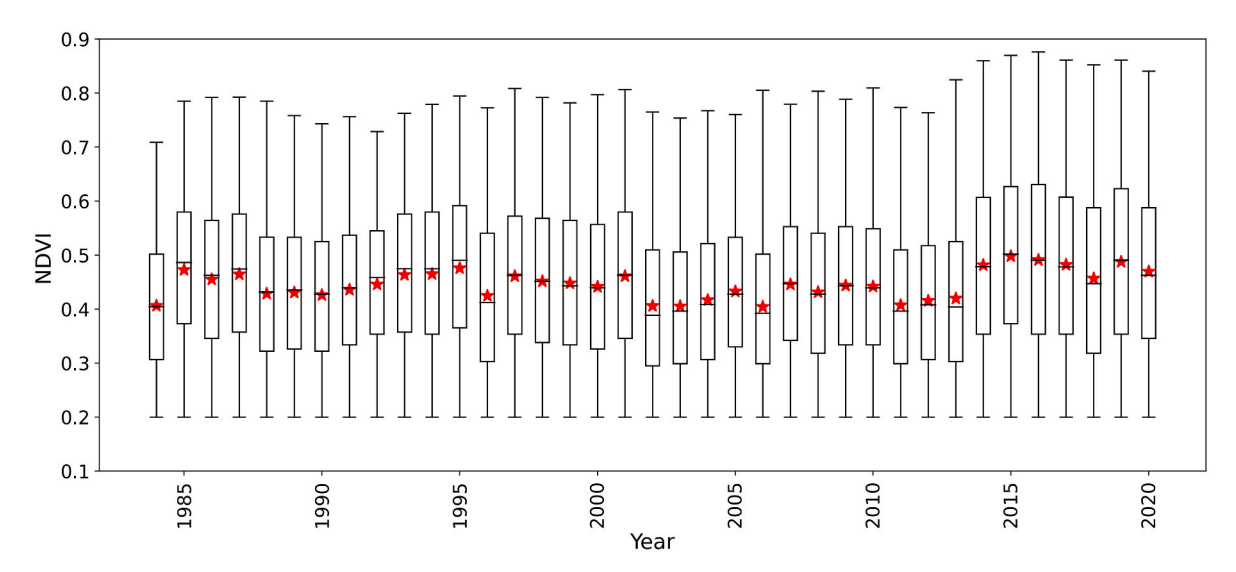


Fig. 4. NDVI for growing season for study reach. Red star represents the mean NDVI. The whisker represents the minimum and maximum value of NDVI, the box height ranges between the 25% quartile (Q1) and 75% quartile (Q3), and the solid middle line represents the median value.

Fig. 6 shows the proportion of vegetation cover, including the proportion of land and water. The vegetated area has increased even though the reach has gone through a long-term extended drought for 20 years since 2000. The proportion of the stream corridor classified as water has decreased. This trend is consistent with field and aerial photograph observations (Fig. 7) along with the development of vegetated sand bars and islands. To elaborate more on change in vegetated area, the percentage change in vegetated area for the entire reach and sub-reaches are also included in the Appendix (Figure A2).

The channel width reduced from an average width of 180 m in 1980 to 90 m in 2020 (Fig. 8). The width was relatively consistent from 1984 to 1998 and then decreased from 2000 to 2020. The minimum channel width was also consistent with time. However, the range of channel width has reduced from 30 to 420 m in 1984 to 30–180 m in 2020.

#### 3.4. Spatial analysis of vegetation and morphology

The changes in spatial patterns of LC were consistent with temporal analysis and revealed the increased vegetation coverage and narrowing of the main channel (Fig. 9). Fig. 9 represents an example of spatial analysis for the sub-section along the Rio Grande. The changes varied spatially and temporally. Fig. 9 shows the increase in riparian vegetation

density, the change in the channel from a single thread to a braided channel, and again to a single thread with a side channel covered by vegetation. This result was consistent with visual observations of channel and vegetation changes (e.g., Fig. 7).

## 3.5. Hydroclimatic variables

The alteration of streamflow obtained from the IHA metrics is represented in Fig. 10. The mean monthly discharge has reduced during the drought (from 2000 to 2020) (Fig. 10A) compared to before 2000. The peak discharge was reduced from 110  $\rm m^3/s$  to 39  $\rm m^3/s$ . The frequency and duration of high pulses decreased, which allowed for vegetation encroachment. Low pulses have also reduced, which is an essential factor for recruiting native vegetation species.

The remaining hydrological variables, including streamflow for the gauging station *below the Cochiti Dam* and climatic variables, are included in the Appendix (Figure A3). The total precipitation was below the average after 2000 (Figure A3 B), and the mean air temperature has increased with time (Figure A3 C) with a fluctuation of estimated reference evapotranspiration (Figure A3 D).

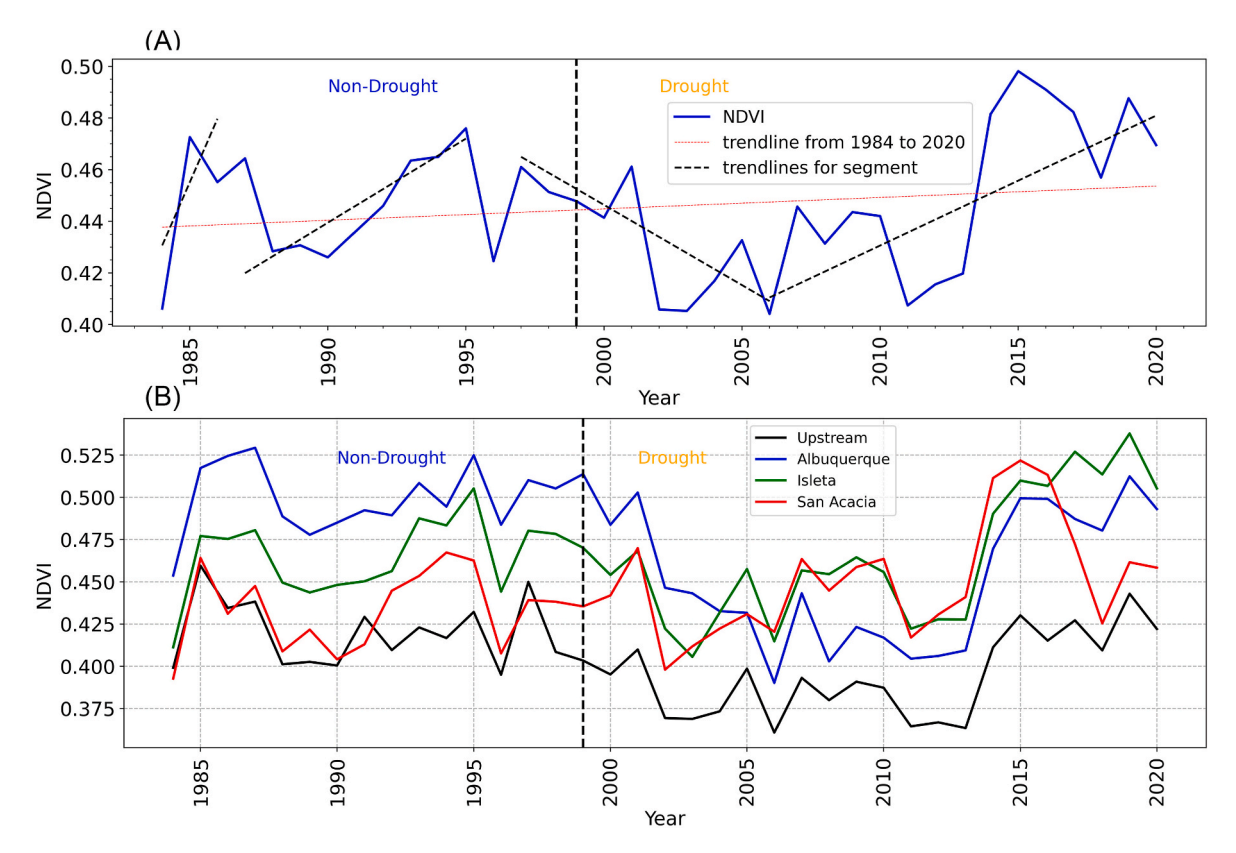


Fig. 5. Annual mean NDVI for the growing season only (A) study reach with trendlines [no significant trend in changing NDVI from 1984 to 2020; from 1984 to 1987, no significant trend; from 1987 to 1995 NDVI, increasing trend; from 1995 to 2006, decreasing trend; and from 2006 to 2020, increasing trend] (B) Sub-reaches.

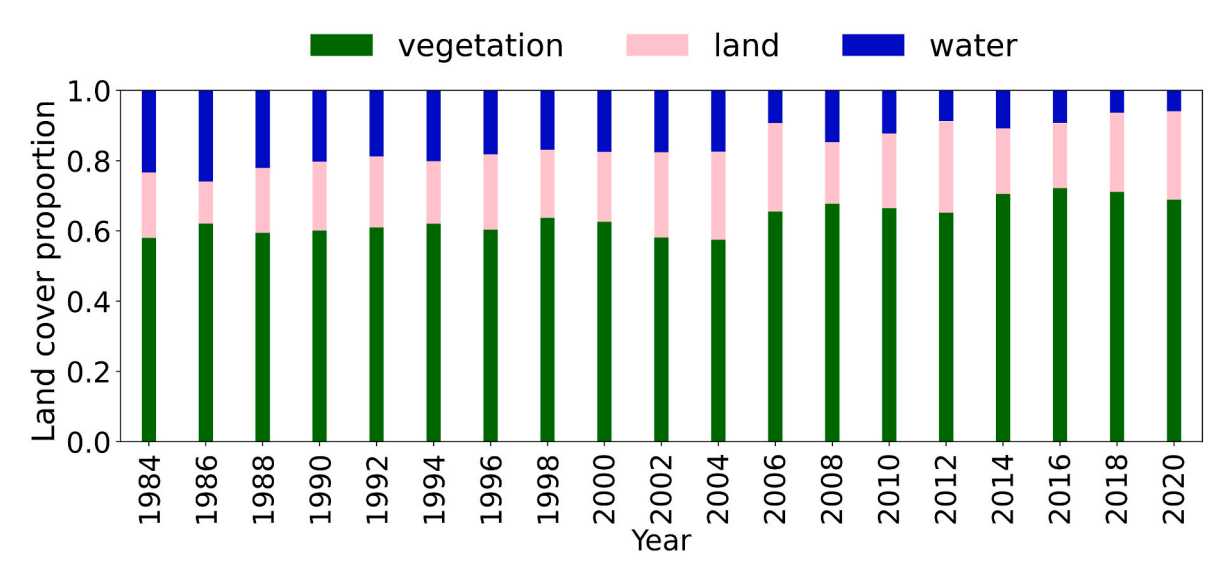


Fig. 6. Proportion of land cover obtained from Random Forest classification for the entire reach.

# 3.6. Correlation between vegetation, morphology, and hydroclimatic variables

A correlation analysis was performed over time (in years) for the four most influential variables obtained from the MDI measure with the dependent variables, NDVI and channel width (Fig. 11). High flow frequency, high flow rise, high pulse count, and minimum air temperature were the four most influential variables for predicting NDVI. In contrast, vegetated area, total precipitation, fall rate, and extreme low duration were most influential in predicting channel width. The figures for MDI

are included in the Appendix (Figure A4). Fig. 11A shows the weak positive correlation of NDVI with all variables except minimum air temperature. However, channel width had a strong positive correlation with precipitation and a negative relation with fall rate (the rate at which the hydrograph recedes), vegetated area, and extreme low duration (Fig. 11B).

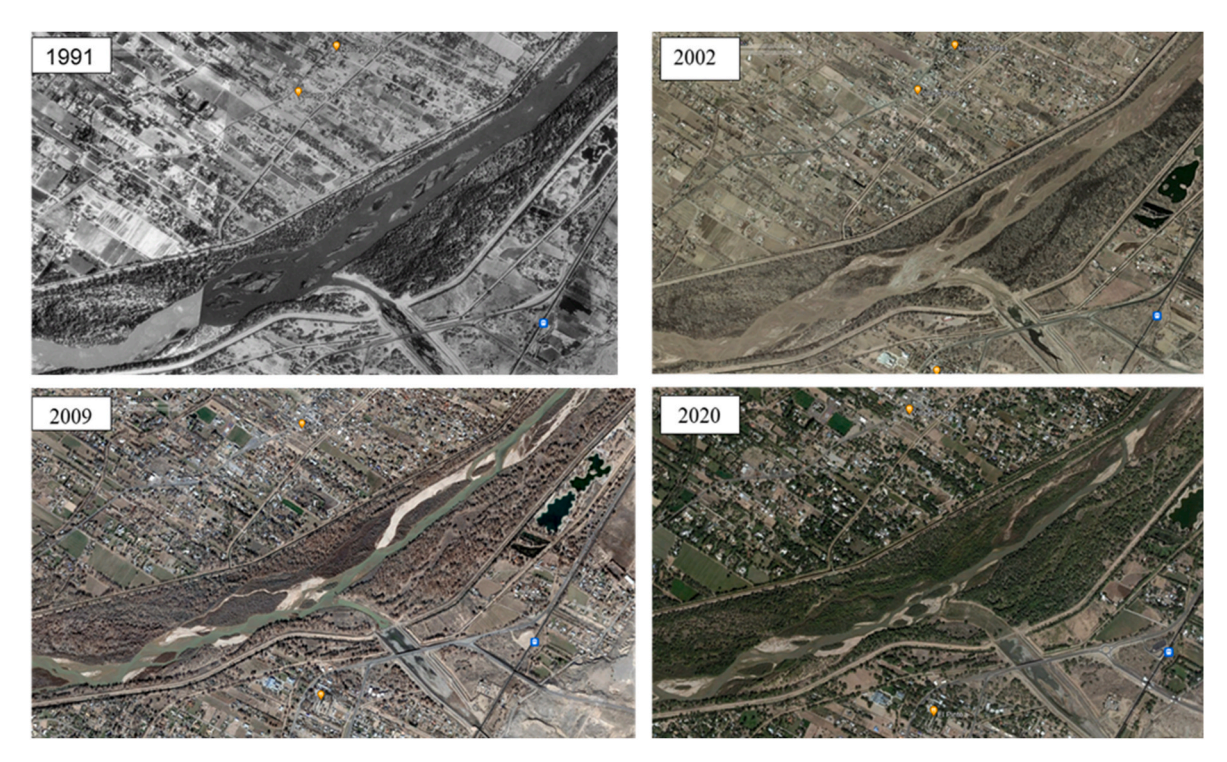


Fig. 7. An example of aerial images for a sub-section representing the change in vegetation density and morphology.

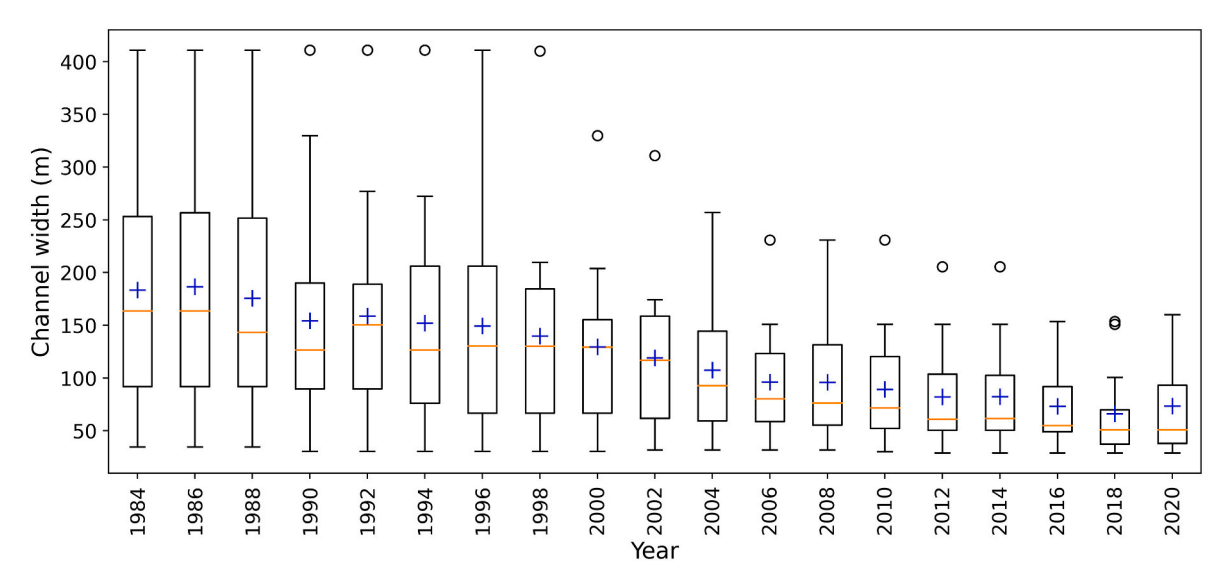


Fig. 8. Channel width from 1984 to 2020 [+ indicates the mean channel width; the box height ranges between the 25% quartile (Q1) and 75% quartile (Q3); the solid middle line represents the median value; the whisker ranges from (Q1-1.5IQR) to (Q3+1.5IQR); IQR = Q3-Q1; and open circles represent the outliers].

## 4. Discussion

# 4.1. Spatiotemporal trends of vegetation and morphology

For arid to semi-arid regions, hydroclimatic variables are the drivers of changes in riparian vegetation and morphology (Stromberg et al., 2010). From 1984 to 1999, the floodplains of the MRG experienced adequate inundation due to overbank flooding (Petrakis et al., 2017) to sustain the riparian vegetation, and high flows contributed to the maintenance of channel width and scouring of vegetation from island and bar features. Severe drought conditions have persisted throughout the Southwestern USA since 2000. The period has been marked by both low precipitation and higher average temperatures (Williams et al.,

2022). All these factors contributed to a substantial reduction in streamflow. High pulses are required to remove encroached vegetation on the banks, islands, and bars. In addition, once vegetation is established, high flows don't generate enough shear stress to remove vegetation (Tetra Tech, 2015). This condition was observed in this study also, in which approximately two years return period of flows in 2005 through the study reach was unable to remove the vegetation from bars and islands to maintain channel width (Chaulagain, 2022). As a result, two major effects are observed: (1) an increase in the vegetated area of the riparian zone; and (2) a reduction in channel width, which is supported by the analysis of our study.

NDVI was reduced during drought and again increased due to vegetation encroachment into the main channel and the formation of



Fig. 9. Spatial analysis for every ten years (A) Land cover and (B) NDVI [NDVI <0 = water, 0-0.2 = land, 0.2-0.5 = sparse and >0.5 = dense vegetation (healthy vegetation)].

vegetated islands and bars even during persistent drought. The decrease in the width of the channel relates to reduced streamflow and an increase in the vegetated area, including the changes in vegetation management (reduced maintenance such as vegetation mowing) due to endangered species recovery efforts. In addition, narrower channels cause the riverbeds to scour for the same reduced streamflow and create a more incised river. In turn, the groundwater table drops, and the

health of the riparian forest is compromised. Endangered species, such as silvery minnow in the case of Rio Grande, lose the habitat of shallow pools they prefer (Archdeacon et al., 2020). Further, as the channel is more incised, it takes a higher flow rate to inundate the vegetated islands. Thus, the river starts to take a different character leading to the invasion of non-native vegetation species resistant to drought (Richardson et al., 2007) and more stable islands (Gurnell et al., 2001).

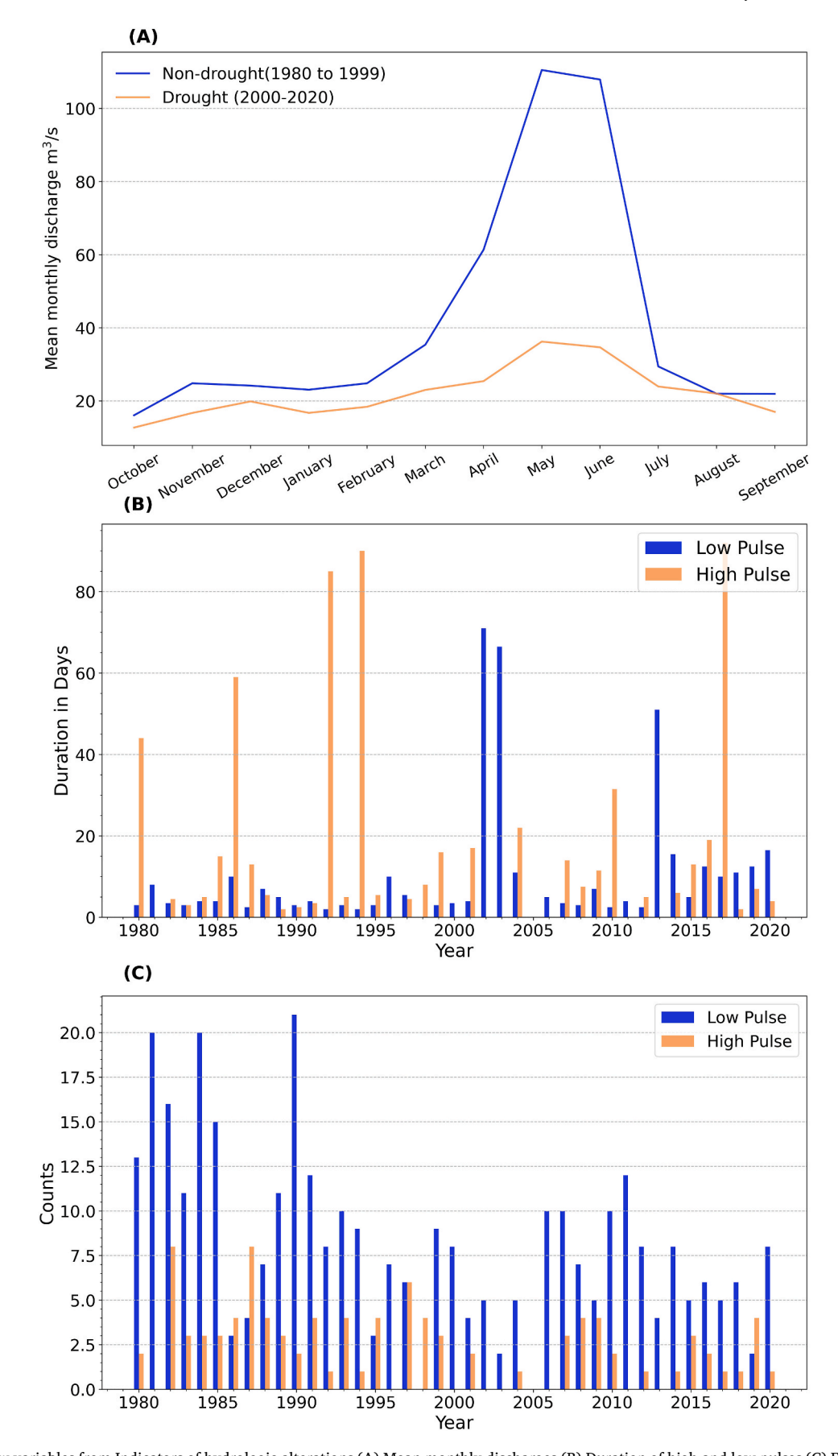
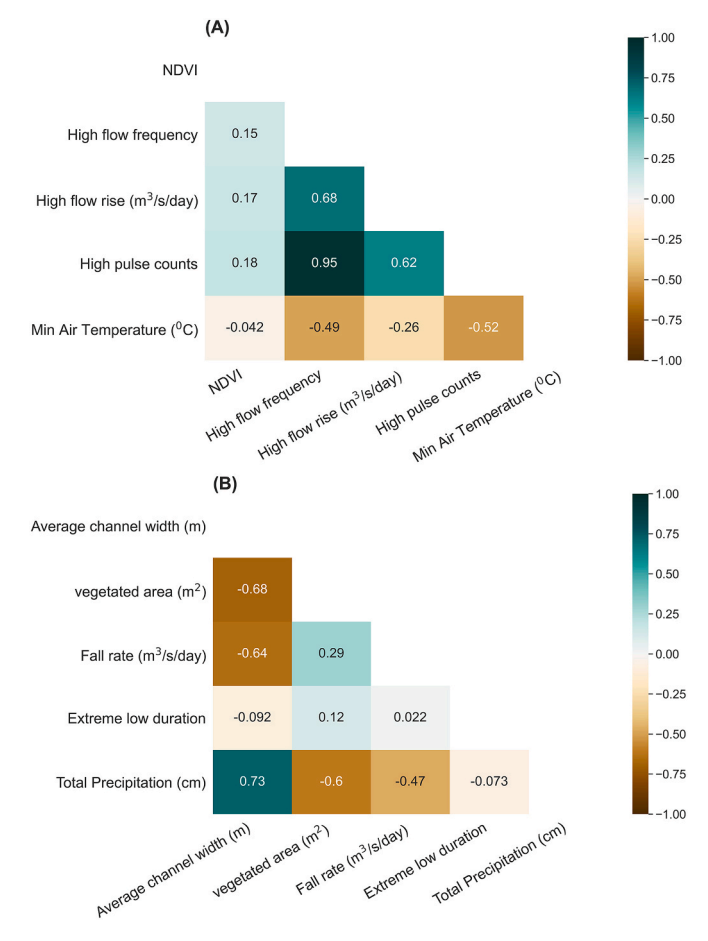


Fig. 10. Stream flow variables from Indicators of hydrologic alterations (A) Mean monthly discharges (B) Duration of high and low pulses (C) Frequency of high and low pulses.



**Fig. 11.** Correlation between **(A)** NDVI with important variables predicted **(B)** Morphology (channel width) with important variables predicted from MDI (numerical values represent Spearman's Rank Correlation Coefficient, a positive value means positive relation and negative means negative relation, closer to  $\pm 1$  (darker shade) means strong relation and closer to 0 (lighter shade) means weaker relation between the variables).

# 4.2. Big data analysis performance

This study successfully performed LC classification and NDVI computation from multi-spectral satellite images in a cloud-based platform using the ML algorithm for large temporal and spatial scales. GEE cloud-based computing platform provides access to big datasets and improves the efficiency of performance in processing time by using a built-in ML algorithm (Gorelick et al., 2017). The same analysis could take longer, making the extensive temporal and spatial scale analysis daunting.

Furthermore, LC classification using the RF algorithm is more accurate than other approaches (Rodriguez-Galiano and Chica-Rivas, 2014). To compare the accuracy of LC for a larger time scale, the availability of ground-truthing data is always a limitation. In this study, some LC mappings were available at different times for specific reach of the study area, which was helpful in verifying the ML approach. The difference in the vegetated area obtained from LC was less than 1% compared to vegetation mapping by Hink and Ohmart, especially for the Albuquerque reach. This reach is densely vegetated and more consistent with time, with fewer disturbances than other reaches. However, wildfires and complete channel desiccation have impacted the San Acacia reach (Fitzner, 2018). The vegetation mapping for 2003 includes the burning evidence for vegetation patches, and some areas have sparse vegetation, which was delineated as vegetation. As a result, there was a larger difference in vegetated areas between the classified LC and ground-truth data.

# 4.3. Correlation between hydroclimatic variables, vegetation, and morphology

Riparian vegetation mostly depends on the streamflow and ground-water for arid or semi-arid regions where precipitation is limited. However, this study was limited to streamflow and climate variables only. This research reveals that the fluctuation of NDVI is weakly correlated with all the climate and streamflow variables. The negative correlation with the minimum air temperature (warmer with time) could be correlated with the negative impacts on the growth of local vegetation species (Weiss et al., 2004) and also due to a reduction in soil moisture. This result was consistent with other studies that have correlated NDVI with temperature in arid or semi-arid regions (Nguyen et al., 2015). Some previous studies found precipitation to be the dominant variable (Wen et al., 2012) that impacts NDVI. However, precipitation was not as influential as streamflow variables for the Rio Grande.

The positive correlation of average channel width with precipitation is due to having enough flows in the river for sediment mobility and removal of encroached vegetation on banks and islands, maintaining channel width. Similarly, vegetation encroachment along the riverbanks can explain the negative correlation of channel width with fall flow rate, extreme low duration, and vegetated area.

#### 4.4. Challenges in using RS images

The characteristics of the MRG led to several challenges in applying RS approaches for LC classification. It is challenging to use medium-resolution images for dynamic rivers similar to MRG. The channel width changed dramatically along San Acacia reach from 1980 to 2020, narrowing to less than 30 m in some places. Using Landsat images to delineate the channel in some parts of the river made it challenging. Also, due to the reduction in river discharge, there was little or no surface flow in the downstream reach during the growing season in recent years. As a result, the channel was misclassified as land, even for high-resolution images (e.g., NAIP imagery). A high degree of supervised training is needed when delineating the channel for turbid, dynamic, and low-flow rivers using images to overcome these limitations.

There are also several limitations in our ability to classify riparian vegetation. Riparian vegetation is the mixture of various vegetation species, from grasses to taller trees (e.g., cottonwoods). In the MRG, mostly willows and Russian olives are found on the river banks. The width covered by these vegetation species is often less than 30 m, which cannot be distinguished using low and medium-resolution images, as was the case for some areas in our study reach. This limits the study of riparian vegetation within narrow riparian corridors. As a result, this study was limited to general vegetation cover rather than a more refined classification. Vegetation species behave differently in response to streamflow characteristics (e.g., high and low flow pulses) and climatic conditions. As a result, vegetation communities can shift from trees and shrubs to grasses or vice versa (Stromberg et al., 2010). In some cases, native vegetation species are replaced by non-native species for altered flows and climate conditions (Richardson et al., 2007). Due to the limitation of the resolution of images, such shifts could not be investigated in this study.

# 4.5. River management implications

The complex interactions between riparian vegetation, channel morphology, and hydroclimatic variables shape rivers and floodplains dynamically. Riparian vegetation impacts the dynamics, forms, and processes of channel morphology (Gurnell, 2014). These changes in the channel and the riparian vegetation can be observed at different spatiotemporal scales. The historical monitoring of the whole reach provides a better understanding of the system. In addition, this enables us to predict the system's behavior in response to similar hydroclimatic conditions. This study has provided valuable information regarding the

changes in riparian vegetation and morphology for a large spatiotemporal scale in relation to hydroclimatic variables in the arid environment that has greater implications on river management such as restoration of riparian vegetation and habitats, in addition to flood management and water delivery. Furthermore, implementing an ML approach for processing the RS products is promising for long-term monitoring of riparian vegetation and channel morphology, which has broader application in a wider range of arid and semi-arid river systems.

In this study, vegetation status in terms of area covered and the NDVI were analyzed based on the streamflow statistics obtained from IHA and climate variables such as temperature and precipitation using simple correlation. However, in future studies, we can quantify the relationship between the streamflow and the climatic variables to understand the dominant factors responsible for a shift in vegetation and channel morphology and the degree of their effects.

## 5. Conclusion

This research aimed to enhance the understanding of riparian vegetation and channel morphology responses to external stressors (hydroclimatic variables) by implementing ML techniques, especially for semi-arid environments. This was accomplished by computing vegetation indices and LC classification obtained from the RF classification in GEE cloud-based storage and computing platform along the MRG. The streamflow and climate variables were correlated with the vegetation status and river morphology. Overall, the vegetated area has increased with fluctuation at different times depending on the hydrology and climatic conditions. The channel has narrowed due to reduced flows and vegetation encroachment. The results also demonstrate that the maintenance of channel width is challenging once the vegetation is established.

The characteristics of the streamflow hydrograph (positive correlation) and air temperature (negative correlation) were dominant among the hydroclimatic variables influencing vegetation cover and channel morphology. The quantification of the relationships between these components with the hydroclimatic variables provides valuable information to understand the nature of impacts and responses due to climate-change-induced drought and engineered infrastructure. This information is essential for river engineers, scientists, and managers regarding river management, such as restoration of riparian vegetation and habitats, including flood management and water delivery. However, using high-resolution images is recommended to perform the vegetation species basis analysis to determine the shift in community composition and density to the changing environment with improved accuracy.

The tools utilized for this research rely on open-source algorithms and cloud-based computing platforms. Thus, the framework of this study is easily applicable on a large spatiotemporal scale for a broader range of arid or semi-arid river systems for the integrated analysis of vegetation and morphology. Overall, this study investigated the existing tools and techniques to improve understanding of river dynamics in large spatiotemporal scales influenced by long-term drought and engineered structures.

# Funding

This work was supported by the National Science Foundation, United States (Awards #1641310 and #2115169).

# CRediT authorship contribution statement

**Smriti Chaulagain:** Conceptualization, Methodology, Software, Writing – original draft, Writing – review & editing, Visualization, Formal analysis. **Mark C. Stone:** Conceptualization, Writing – review & editing, Supervision, Funding acquisition. **Ryan R. Morrison:** Conceptualization, Supervision, Writing – review & editing. **Liping Yang:** Conceptualization, Validation, Writing – review & editing. **Julie** 

**Coonrod:** Conceptualization, Writing – review & editing. **Noelani E. Villa:** Writing – review & editing.

## **Declaration of competing interest**

The authors declare that they have no known competing financial interests or personal relationships that could have appeared to influence the work reported in this paper.

#### Data availability

We have shared the link and codes in attached manuscript.

AbbreviationsFor readability, below, we provide a list of abbreviations (ordered alphabetically) used in our article.

GEE Google Earth Engine

IHA Indicators of Hydrologic Alterations

LC Land cover

LiDAR Light Detection and Ranging
MDI Mean Decrease Impurity
ML Machine learning

MNDWI Modified Normalized Difference Water Index MODIS Moderate Resolution Imaging Spectroradiometer

MRG Middle Rio Grande

NAIP National Agriculture Imagery Program
NDVI Normalized Difference Vegetation Index

OA Overall accuracy RF Random Forest RS Remote Sensing USA United States

USBOR United States Bureau of Reclamation

# Appendix A. Supplementary data

Supplementary data to this article can be found online at https://doi.org/10.1016/j.jaridenv.2023.105068.

### References

Archdeacon, T.P., Diver-Franssen, T.A., Bertrand, N.G., Grant, J.D., 2020. Drought results in recruitment failure of Rio Grande silvery minnow (Hybognathus amarus), an imperiled, pelagic broadcast-spawning minnow. Environ. Biol. Fish. 103 (9), 1033–1044. https://doi.org/10.1007/s10641-020-01003-5.

Artini, G., Calvani, G., Francalanci, S., Solari, L., 2021. Effects of Vegetation at a Bar Confluence on River Hydrodynamics: the Case Study of the Arno River at Greve Junction. River Research and Applications. https://doi.org/10.1002/rra.3774 rra.3774.

Assal, T.J., Steen, V.A., Caltrider, T., Cundy, T., Stewart, C., Manning, N., Anderson, P.J., 2021. Monitoring long-term riparian vegetation trends to inform local habitat management in a mountainous environment. Ecol. Indicat. 127, 107807 https://doi. org/10.1016/j.ecolind.2021.107807.

Bertoldi, W., Welber, M., Gurnell, A.M., Mao, L., Comiti, F., Tal, M., 2015. Physical modelling of the combined effect of vegetation and wood on river morphology. Geomorphology 246, 178–187. https://doi.org/10.1016/j.geomorph.2015.05.038.

Bollati, I.M., Pellegrini, L., Rinaldi, M., Duci, G., Pelfini, M., 2014. Reach-scale morphological adjustments and stages of channel evolution: the case of the Trebbia River (northern Italy). Geomorphology 221, 176–186. https://doi.org/10.1016/j. geomorph.2014.06.007.

Boothroyd, R.J., Nones, M., Guerrero, M., 2021a. Deriving planform morphology and vegetation coverage from remote sensing to support river management applications. Front. Environ. Sci. 9, 657354 https://doi.org/10.3389/fenvs.2021.657354.

Boothroyd, R.J., Williams, R.D., Hoey, T.B., Barrett, B., Prasojo, O.A., 2021b.

Applications of Google Earth Engine in fluvial geomorphology for detecting river channel change. WIREs Water 8 (1). https://doi.org/10.1002/wat2.1496.

Brierley, G.J., Cohen, T., Fryirs, K., Brooks, A., 1999. Post-European changes to the fluvial geomorphology of Bega catchment, Australia: implications for river ecology. Freshw. Biol. 41 (4), 839–848. https://doi.org/10.1046/j.1365-2427.1999.00397.x.

Calle, M.L., Urrea, V., 2011. Letter to the editor: stability of random forest importance measures. Briefings Bioinf. 12 (1), 86–89. https://doi.org/10.1093/bib/bbq011.

Caruso, B.S., Pithie, C., Edmondson, L., 2013. Invasive riparian vegetation response to flow regimes and flood pulses in a braided river floodplain. J. Environ. Manag. 125, 156–168. https://doi.org/10.1016/j.jenvman.2013.03.054.

- Chaulagain, S., 2022. An Investigation of Emerging Technologies to Advance the Understanding of Dynamics between the Floodplain and Main Channel Due to Riparian Vegetation. University of New Mexico.
- Chi, K., Pang, B., Cui, L., Peng, D., Zhu, Z., Zhao, G., Shi, S., 2020. Modelling the vegetation response to climate changes in the Yarlung Zangbo river basin using Random Forest. Water 12 (5), 1433. https://doi.org/10.3390/w12051433.
- Fitzner, A., 2018. Middle Rio Grande Project Albuquerque Area Office Upper Colorado Region. U.S. Department of the Interior Bureau of Reclamation.
- Foody, G.M., 2020. Explaining the unsuitability of the kappa coefficient in the assessment and comparison of the accuracy of thematic maps obtained by image classification. Rem. Sens. Environ. 239, 111630 https://doi.org/10.1016/j. res. 2010.111630
- Gorelick, N., Hancher, M., Dixon, M., Ilyushchenko, S., Thau, D., Moore, R., 2017. Google Earth engine: planetary-scale geospatial analysis for everyone. Rem. Sens. Environ. 202, 18–27. https://doi.org/10.1016/j.rse.2017.06.031.
- Gurnell, A., 2014. Plants as river system engineers: plants as river system engineers. Earth Surf. Process. Landforms 39 (1), 4–25. https://doi.org/10.1002/esp.3397.
- Gurnell, A.M., Petts, G.E., Hannah, D.M., Smith, B.P.G., Edwards, P.J., Kollmann, J., Ward, J.V., Tockner, K., 2001. Riparian vegetation and island formation along the gravel-bed Fiume Tagliamento, Italy. Earth Surf. Process. Landforms 26 (1), 31–62. https://doi.org/10.1002/1096-9837(200101)26:1<31::AID-ESP155>3.0.CO;2-Y.
- Hamed, K.H., Ramachandra Rao, A., 1998. A modified Mann-Kendall trend test for autocorrelated data. J. Hydrol. 204 (1), 182–196. https://doi.org/10.1016/S0022-1694(97)00125-X.
- Han, M., Brierley, G., Li, B., Li, Z., Li, X., 2020. Impacts of flow regulation on geomorphic adjustment and riparian vegetation succession along an anabranching reach of the Upper Yellow River. Catena 190, 104561. https://doi.org/10.1016/j. catena.2020.104561.
- Hussain, M.M., Mahmud, I., 2019. pyMannKendall: a python package for non parametric Mann Kendall family of trend tests. J. Open Source Softw. 4 (39), 1556. https://doi. org/10.21105/joss.01556.
- Isikdogan, F., Bovik, A.C., Passalacqua, P., 2017. Surface water mapping by deep learning. IEEE J. Sel. Top. Appl. Earth Obs. Rem. Sens. 10 (11), 4909–4918. https://doi.org/10.1109/JSTARS.2017.2735443.
- Johansen, K., Phinn, S., Witte, C., 2010. Mapping of riparian zone attributes using discrete return LiDAR, QuickBird and SPOT-5 imagery: assessing accuracy and costs. Rem. Sens. Environ. 114 (11), 2679–2691. https://doi.org/10.1016/j. rse.2010.06.004.
- Knox, R.L., Morrison, R.R., Wohl, E.E., 2022. A river ran through it: floodplains as America's newest relict landform. Sci. Adv. 8 (25), eabo1082 https://doi.org/ 10.1126/sciady.abo1082.
- Langat, P.K., Kumar, L., Koech, R., 2019. Monitoring river channel dynamics using remote sensing and GIS techniques. Geomorphology 325, 92–102. https://doi.org/ 10.1016/j.geomorph.2018.10.007.
- Maxwell, A.E., Strager, M.P., Warner, T.A., Ramezan, C.A., Morgan, A.N., Pauley, C.E., 2019. Large-area, high spatial resolution land cover mapping using Random Forests, GEOBIA, and NAIP Orthophotography: findings and recommendations. Rem. Sens. 11 (12), 12 https://doi.org/10.3390/rs11121409.
- Monegaglia, F., Zolezzi, G., Güneralp, I., Henshaw, A.J., Tubino, M., 2018. Automated extraction of meandering river morphodynamics from multitemporal remotely sensed data. Environ. Model. Software 105, 171–186. https://doi.org/10.1016/j. envsoft.2018.03.028.
- Mussetter Engineering, Inc, 2006. Evaluation of Bar Morphology, Distribution and Dynamics as Indices of Fluvial Processes in the Middle Rio Grande (New Mexico).
- Nagler, P.L., Doody, T.M., Glenn, E.P., Jarchow, C.J., Barreto-Muñoz, A., Didan, K., 2016. Wide-area estimates of evapotranspiration by red gum (*Eucalyptus camaldulensis*) and associated vegetation in the murray-darling river basin, Australia: wide-area estimates of evapotranspiration by red gum. Hydrol. Process. 30 (9), 1376–1387. https://doi.org/10.1002/hyp.10734.
- Ndayisaba, F., Guo, H., Isabwe, A., Bao, A., Nahayo, L., Khan, G., Kayiranga, A., Karamage, F., Muhire, E.N., 2017. Inter-annual vegetation changes in response to climate variability in Rwanda. J. Environ. Protect. 8 (4) https://doi.org/10.4236/ jep.2017.84033. Article 4.
- Nepf, H.M., 2012. Hydrodynamics of vegetated channels. J. Hydraul. Res. 50 (3), 262–279. https://doi.org/10.1080/00221686.2012.696559.
- Nguyen, U., Glenn, E.P., Nagler, P.L., Scott, R.L., 2015. Long-term decrease in satellite vegetation indices in response to environmental variables in an iconic desert riparian ecosystem: the Upper San Pedro, Arizona, United States: decrease in vegetation indices: san pedro river. Ecohydrology 8 (4), 610–625. https://doi.org/10.1002/ eco.1529.

- Petrakis, R., van Leeuwen, W., Villarreal, M.L., Tashjian, P., Dello Russo, R., Scott, C., 2017. Historical analysis of riparian vegetation change in response to shifting management objectives on the Middle Rio Grande. Land 6 (2), 29. https://doi.org/ 10.3390/land6020029
- Phan, T.N., Kuch, V., Lehnert, L.W., 2020. Land cover classification using Google Earth Engine and Random Forest classifier—the role of image composition. Rem. Sens. 12 (15), 2411. https://doi.org/10.3390/rs12152411.
- Picco, L., Comiti, F., Mao, L., Tonon, A., Lenzi, M.A., 2017. Medium and short term riparian vegetation, island and channel evolution in response to human pressure in a regulated gravel bed river (Piave River, Italy). Catena 149, 760–769. https://doi. org/10.1016/j.catena.2016.04.005.
- Poff, N.L., Olden, J.D., Merritt, D.M., Pepin, D.M., 2007. Homogenization of regional river dynamics by dams and global biodiversity implications. Proc. Natl. Acad. Sci. USA 104 (14), 5732–5737. https://doi.org/10.1073/pnas.0609812104.
- Pu, G., Quackenbush, L.J., Stehman, S.V., 2021. Using Google Earth Engine to assess temporal and spatial changes in river geomorphology and riparian vegetation. JAWRA J. Am.Water Resour. Associat. https://doi.org/10.1111/1752-1688.12950, 1752-1688.12950.
- Richardson, D.M., Holmes, P.M., Esler, K.J., Galatowitsch, S.M., Stromberg, J.C., Kirkman, S.P., Pyšek, P., Hobbs, R.J., 2007. Riparian vegetation: degradation, alien plant invasions, and restoration prospects: riparian vegetation: degraded, invaded, transformed. Divers. Distrib. 13 (1), 126–139. https://doi.org/10.1111/j.1366-9516-2006-00314 x
- Richter, B.D., Baumgartner, J.V., Powell, J., Braun, D.P., 1996. A method for assessing hydrologic alteration within ecosystems. Conserv. Biol. 10 (4), 1163–1174. https:// doi.org/10.1046/j.1523-1739.1996.10041163.x.
- Rodriguez-Galiano, V.F., Chica-Rivas, M., 2014. Evaluation of different machine learning methods for land cover mapping of a Mediterranean area using multi-seasonal Landsat images and Digital Terrain Models. Int. J.Dig.Earth 7 (6), 492–509. https://doi.org/10.1080/17538947.2012.748848.
- Schwenk, J., Khandelwal, A., Fratkin, M., Kumar, V., Foufoula-Georgiou, E., 2017. High spatiotemporal resolution of river planform dynamics from Landsat: the RivMAP toolbox and results from the Ucayali River. Earth Space Sci. 4 (2), 46–75. https:// doi.org/10.1002/2016EA000196.
- Sims, N.C., Colloff, M.J., 2012. Remote sensing of vegetation responses to flooding of a semi-arid floodplain: implications for monitoring ecological effects of environmental flows. Ecol. Indicat. 18, 387–391. https://doi.org/10.1016/j.ecolind.2011.12.007.
- Stromberg, J.C., Lite, S.J., Dixon, M.D., 2010. Effects of stream flow patterns on riparian vegetation of a semi-arid river: implications for a changing climate: effects of stream flow patterns. River Res. Appl. 26 (6), 712–729. https://doi.org/10.1002/rra.1272.
- Swanson, B.J., Meyer, G.A., Coonrod, J.E., 2011. Historical channel narrowing along the Rio Grande near Albuquerque, New Mexico in response to peak discharge reductions and engineering: magnitude and uncertainty of change from air photo measurements. Earth Surf. Process. Landforms 36 (7), 885–900. https://doi.org/ 10.1002/esp.2119.
- Tech, Tetra, 2015. Elm Creek Flow-Sediment-Mechanical Adaptive Management Experiment Final Report. Tetra Tech, Fort Collins.
- Türk, G., 1979. Gt index: a measure of the success of prediction. Rem. Sens. Environ. 8 (1), 65–75. https://doi.org/10.1016/0034-4257(79)90024-5.
- Weiss, J.L., Gutzler, D.S., Allred Coonrod, J.E., Dahm, C.N., 2004. Seasonal and interannual relationships between vegetation and climate in central New Mexico, USA. J. Arid Environ. 57 (4), 507–534. https://doi.org/10.1016/S0140-1963(03)00113-7
- Wen, L., Yang, X., Saintilan, N., 2012. Local climate determines the NDVI-based primary productivity and flooding creates heterogeneity in semi-arid floodplain ecosystem. Ecol. Model. 242, 116–126. https://doi.org/10.1016/j.ecolmodel.2012.05.018.
- Williams, A.P., Cook, B.I., Smerdon, J.E., 2022. Rapid intensification of the emerging southwestern North American megadrought in 2020–2021. Nat. Clim. Change 15.
- Yang, L., Cervone, G., 2019. Analysis of remote sensing imagery for disaster assessment using deep learning: a case study of flooding event. Soft Comput. https://doi.org/ 10.1007/s00500-019-03878
- Yonaba, R., Biaou, A.C., Koïta, M., Tazen, F., Mounirou, L.A., Zouré, C.O., Queloz, P., Karambiri, H., Yacouba, H., 2021a. A dynamic land use/land cover input helps in picturing the Sahelian paradox: assessing variability and attribution of changes in surface runoff in a Sahelian watershed. Sci. Total Environ. 757, 143792 https://doi. org/10.1016/j.scitotenv.2020.143792.
- Yonaba, R., Koïta, M., Mounirou, L.A., Tazen, F., Queloz, P., Biaou, A.C., Niang, D., Zouré, C., Karambiri, H., Yacouba, H., 2021b. Spatial and transient modelling of land use/land cover (LULC) dynamics in a Sahelian landscape under semi-arid climate in northern Burkina Faso. Land Use Pol. 103, 105305 https://doi.org/10.1016/j. landusepol.2021.105305.